ACS MATERIALS LETTERS

www.acsmaterialsletters.org

From Brittle to Ductile: Symmetry Breaking in Strut-Based Architected Materials

Shao-Yi Yu, Sangryun Lee, Zhizhou Zhang, Zeqing Jin, and Grace X. Gu*

Cite This: *ACS Materials Lett.* 2023, 5, 1288–1294

Read Online

ACCESS | Metrics & More | Article Recommendations | Supporting Information

ABSTRACT: **Strut-based cellular structures have gained remarkable attention in recent years due to their improved strength-to-weight ratio, energy absorption abilities, and heat transfer properties. A key feature of cellular structures employed in modern infrastructure and devices is a symmetric configuration with repeating unit cells. This periodic design makes fabrication more feasible for next-generation aerospace and biomedical materials. However, such a design with brittle constituents often undergoes a sudden and catastrophic failure as all unit cells along a fracture surface tend to fail simultaneously at a critical loading condition. In this paper, we propose an elegant solution to achieve progressive failure by adjusting the diameter of each strut to create asymmetric or irregular cellular structures. Finite element simulations are conducted and validated by comparing with experiments on additively manufactured samples. Designs are then categorized into three failure modes and the relationship between the failure modes and the stress−strain curves are analyzed. Lastly, simulation-based Bayesian optimization is applied to design the structures with a more distributed stress field before failure and therefore improve their strength and energy absorption capabilities. Results show that the proposed designs fail at the boundaries and the cracks grow locally without penetrating through the entire structure, leading to more progressive failure. This research proposes novel cellular structures via symmetry breaking to achieve structures with promising manufacturability and damage-tolerant failure, greatly broadening their applications.**

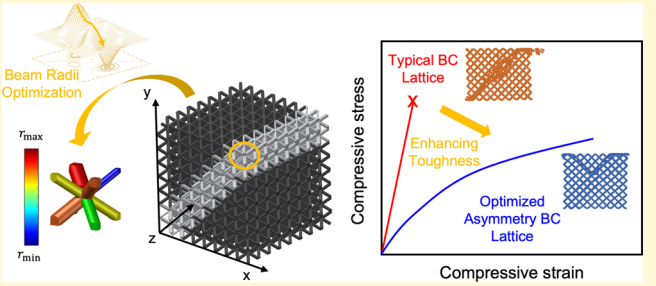

Cellular structures, types of porous materials, are prevalent as building blocks in nature, such as cork, sponge, and trabecular bone.[1,2] These structures with open-cell arrangements are referred to as lattice structures and are oftentimes lauded for their high strength/stiffness-to-weight ratio and enhanced energy absorption abilities.[3−6] For instance, these properties are beneficial to the aircraft fuselage since interior sandwich panels made with cellular materials as core structures can increase the critical loads that an aircraft can bear after being hit by birds or debris.[7] Cellular structures can also be used in designing implant biomedical devices for their biomimetic features that can provide stability[8] or be used as a substrate matrix for growing cells. Therefore, researchers have been pushing the boundaries in developing these multifunctional materials with improved mechanical properties. A common feature of cellular structures employed in modern engineering applications is a symmetric configuration of repeating unit cells. The main benefits of using repeating unit cells are a greatly reduced design space and higher generalizability to more complex parts. This feature, however, poses a drawback in the case of brittle constituents: when one unit cell fails, the other unit cells will successively fail under critical compression loading, causing a sudden and catastrophic failure in the structure.[3] This detrimental failure mode prevents early detection of failure, prompting the development of asymmetric cellular materials, which are materials consisting of heterogeneous microstructures.[9−12]

Research aimed at mimicking the microscale features of crystalline structures has been proposed to develop architected materials with higher toughness by leveraging different fracture toughening mechanisms, such as grain boundaries, precipitates, and phases.[13,14] Some research aimed at designing graded structures with different relative density distributions within the design domain.[15−17] Several methods are also used to create heterostructures, such as applying the Voronoi diagram to the original reference points to rearrange a regular hexagonal honeycomb structure,[10] using multiobjective topology opti-

Received: January 2, 2023
Accepted: March 22, 2023
Published: March 27, 2023

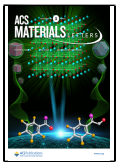

Downloaded via UNIV OF CALIFORNIA BERKELEY on September 8, 2023 at 22:26:47 (UTC).
See https://pubs.acs.org/sharingguidelines for options on how to legitimately share published articles.

ACS Publications

© 2023 American Chemical Society

https://doi.org/10.1021/acsmaterialslett.3c00002
ACS Materials Lett. 2023, 5, 1288−1294

mization under fixed volume constraint to generate networked structures,[18] stacking two materials with different microstructures,[19] or constructing material foams.[20] However, most of the current approaches for creating asymmetric cellular structures can overly complicate the modeling and manufacturing processes as they often use sophisticated unit cell arrangements or large amounts of input parameters. A knowledge gap also exists in understanding how to manipulate the architecture and deformation behaviors of asymmetric cellular structures to better balance the trade-off between strength and toughness, which is often seen in engineering materials.

Therefore, in this study, we propose a de novo method for creating asymmetric cellular structures by designing the spatial distribution patterns and variance of the beam elements' radius near the fracture surface for enhanced mechanical properties. The proposed method not only significantly broadens the design space with only 16 design variables and consistent unit cell structure but also formulates the design process into a constrained optimization problem. We examine the local behaviors of each beam element and its contribution to the global mechanical properties and failure mode of architected materials. Since beams with different radii have different tolerances to bear the external loadings, an architected material can be designed to have progressive failure despite having brittle constituents. This study leads to the discovery of highly versatile material designs without catastrophic failures and complications in manufacturing compared with conventional engineering counterparts, opening up unexplored possibilities in the fields that can greatly broaden the applications of cellular structural materials.

Asymmetric Cellular Structures. Here, we aim to design asymmetric body-centered (BC) cellular structures that fail progressively by using different strut radii to manipulate the crack propagation during compression, as shown in Figure 1(A). The reason for choosing BC unit cells is that these structures tend to experience more catastrophic failure due to the stress concentrations of the bending force near the joints.[3] However, in our designs, it is hypothesized that struts with different radii have different tolerance to external loads. Therefore, unlike conventional BC structures, which share an identical failure path, asymmetric designs with appropriate struts arrangements are expected to hinge and guide crack propagation for more ductile failure. In this way, we can create designs with the ability to hold external loading during the failure, leading to more ductile stress−strain curves with higher toughness and more progressive failure behavior. The design domain of interest is a structure with 512 unit cells (8 by 8 by 8) to ensure the convergence of the global materials properties and the edge lengths are 10 mm. As shown in Figure 1(A), we modify the radii of the tridiagonal beams colored in the figure in the $x-y$ plane while keeping the designs along the z axis identical. Since there are 16 beams lying along the main diagonal, 15 beams lying under and above them, and so on, we can sum all the beams within the tridiagonal range, leading to a total of 100 beams. During the design process, the radii of those beams are varied, and this results in 100 design variables for the entire structure. By doing so, the asymmetric structures are expected to fail more progressively compared to their symmetric counterpart as shown in the figure. In order to further validate our hypothesis that varying beam radii can result in different mechanical properties and failure modes, we develop a finite element model and 3D print the samples, using

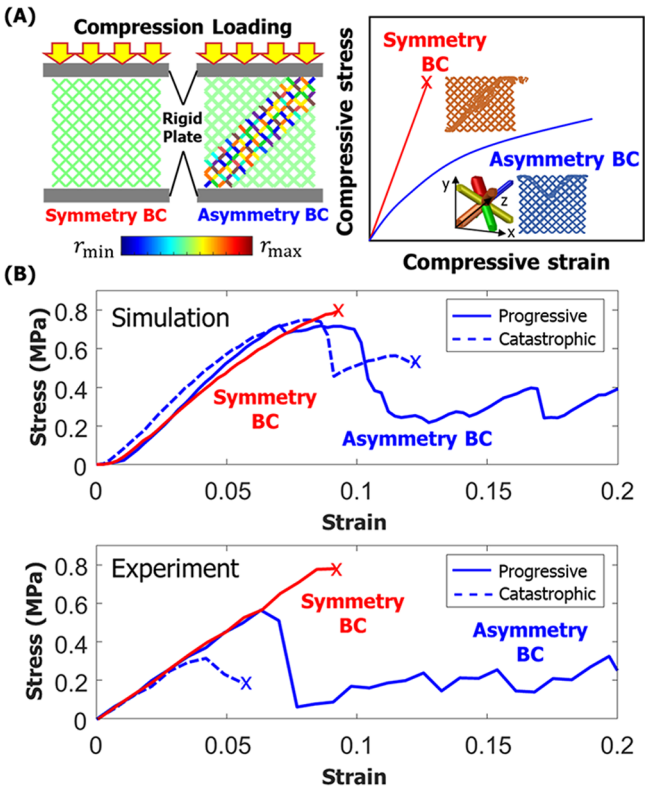

Figure 1. Loading and symmetry conditions with results from simulation and experiment. (A) The schematic of the cellular structures under compression loads shows the experimental and simulation setup and the expected difference between symmetric and asymmetric BC structures. (B) Simulation and experimental stress−strain curves of the cellular structures, validating our design hypothesis that the introduced design variables can lead to distinct failure modes. The solid line represents the progressive failure while the dashed line shows the catastrophic failure.

a stereolithography (SLA) printer, to conduct uniaxial compression tests from which we obtain the homogenized strength and toughness of the structures. Simulation and experimental details are described in the Methods Section. As shown in Figure 1(B), even though there exist deviations in the values between experimental and simulation results, the stress−strain curves show similar trends in failure behaviors. It is hypothesized that the deviation may be caused by the potential defects in the fabricated samples while removing the support materials and the directionality from the nature of the 3D printing process. The solid line represents the progressive failure while the dashed line shows the catastrophic failure. From the figure, it can be seen that the proposed method can create asymmetric structures with distinct failure behaviors. Furthermore, by randomly assigning radii on tridiagonal beams, it is possible to create designs with more ductile macroscopic failure behaviors compared to conventional symmetric designs. However, this large number of variables is impractical for the design since there are redundant parameters that does not affect much the targeted mechanical properties.

To eliminate the design variables that have less control to the performance so that the designs can be augmented with fewer variables, we design the structures using 16 variables. Figure 2(A) shows the design process. First, 8 beam radii are sampled from a uniform distribution within 0.5 to 1.7 mm. The

https://doi.org/10.1021/acsmaterialslett.3c00002
ACS Materials Lett. 2023, 5, 1288−1294

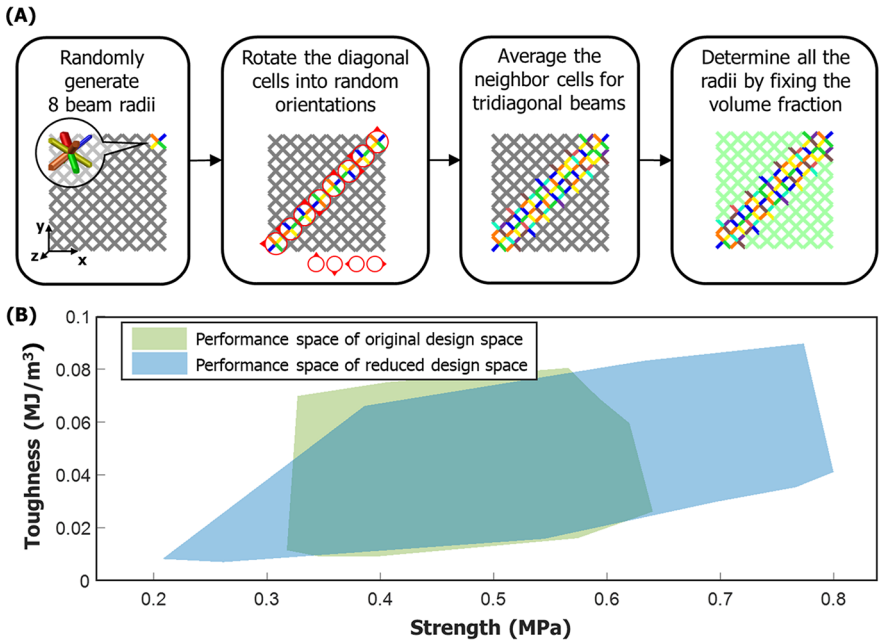

Figure 2. Design process and comparison of full and reduced design spaces. (A) The design process of the asymmetric cellular structures using 16 parameters. (B) The comparison of the Ashby chart between original (100 parameters) and reduced design spaces (16 parameters).

lower bound is set due to the resolution of the 3D printer and the upper bound is used to constrain the size of the unit cell. Then 8 identical unit cells are randomly assigned to one of six different orientations and are positioned along the diagonal. By using this method, 8 unit cells with different beam radii are effectively created with 16 parameters. To further diversify the beams and increase the irregularity without introducing new variables, we average the beams in the neighbor cells along the diagonal to construct tridiagonal beams. Lastly, the radii of the rest of the beams are determined by fixing the volume fraction of all the designs to 0.2. The structures are all the same along the *z*-direction for simplicity. We examine the distribution of the designs under 16 variables on the Ashby chart and find that this design space can still cover a large enough performance space as shown in Figure 2(B). Therefore, these 16 parameters, including 8 beam radii and 8 orientations for each diagonal unit cell, are used to design the structures.

Failure Modes under Compression Loads. We have generated 355 designs from uniform distributions and run batch simulations to obtain their stress−strain curves. Supporting Information Figure S1 shows the distribution remains similar across varying numbers of data points drawn from a uniform distribution. Simulation details are described in the Methods Section. The structures are considered to be failed when the stress drops below 0.1 MPa for the first time since the experiments are not under perfect displacement control, and the effect of the threshold stress values can be found in the Supporting Information Figure S2. Strength is denoted as the first peak stress on the curves while toughness is the area under the curves before the structure fails. Figure 3 shows the Ashby chart for all the designs; the strength ranges widely from 0.2 to around 0.8 MPa, while the toughness for most of the designs falls below 0.05 MJ/m^3. There exists a positive correlation between strength and toughness of these asymmetric structures, which is not usually seen in an engineering material. From inspecting the failure sequences of the beams and how the cracks propagate within the

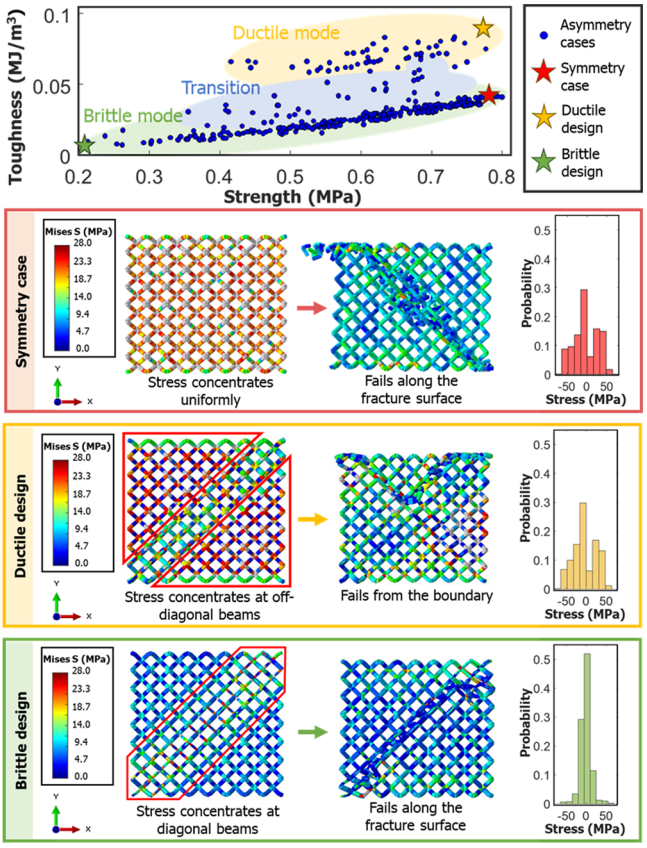

Figure 3. Simulation-based Ashby chart of the asymmetric cellular structures. This figure shows failure modes and local stress distribution of different structures. The asymmetric structures can be further categorized into ductile, transition, and brittle modes. The histograms show the stress distribution within the structures right before the structures fail.

https://doi.org/10.1021/acsmaterialslett.3c00002
ACS Materials Lett. 2023, 5, 1288−1294

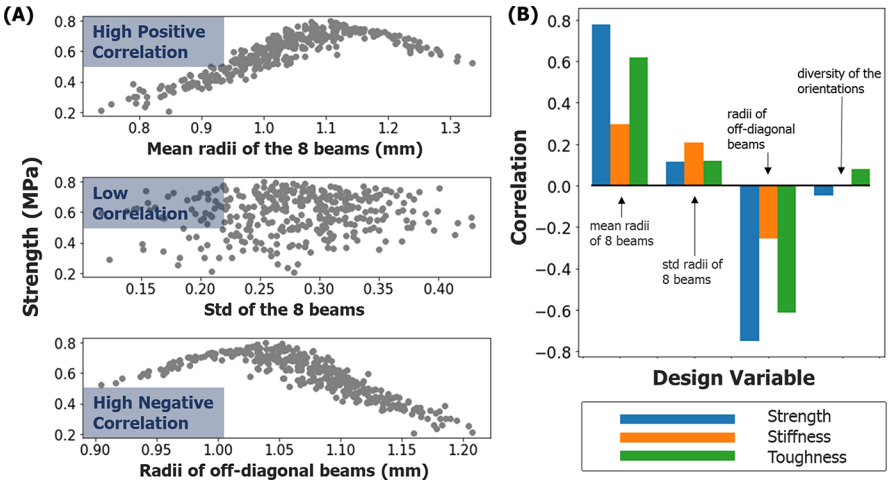

Figure 4. Correlation between different design variables and material properties. (A) How strength varies under different design parameters. Each point on the plot is a single design. (B) The correlations of design variables and the mechanical properties.

structures, we can categorize these structures into three failure modes: brittle mode, transition, and ductile mode. The designs in the brittle mode fail catastrophically with clear fracture surfaces along the diagonal and therefore have lower toughness, which is less desired in most applications. One of the representative cases of this category is the symmetric cellular structure. Due to the identical unit cells in symmetric cellular structure, the stress distributes uniformly within the structure before failure, leading to the existence of higher strength compared to other brittle mode structures. In other brittle mode structures, thinner struts near the diagonal surface, which are incapable of holding shear stress, result in more uneven stress distribution during the compression and lead to both low strength and toughness. On the other hand, ductile mode structures tend to break from the weakest part, at the boundaries or where thin struts are located, but the cracks are unable to propagate throughout the structures. This is because stress of the ductile mode structures often concentrate on off-diagonal beams at the beginning of the compression. As the shear stress builds up along the diagonal, the stress can distribute more uniformly before the structures fail. These designs often have higher toughness and are more desired in the applications with broader usage. To conclude, we can see that, as shown in Figure 3, the stress field of ductile design is more distributed compared to a brittle design. The distributed stress field could be obtained by tuning the radii of each strut and the stress concentrated at off-diagonal beams whereas the brittle design has a highly concentrated stress field at diagonal beams, which result in catastrophic failure as observed in both our simulations and experiments. The snapshots of the simulations are provided in the Supporting Information Figures S3–S5 to demonstrate the failure behaviors of the designs. However, there is no clear line between brittle and ductile modes. Instead, we observe a transition zone between brittle and ductile modes. Transition includes the structures whose failure modes cannot be easily categorized as brittle or ductile and often have cracks propagating relatively slowly along the diagonal fracture surfaces (brittle mode) and locally beam failure near the boundaries (ductile mode). It is worth noting that 86.48% of the 355 designs drawn from the uniform distribution fall into brittle or transition modes while only a few designs are categorized as ductile. From the stress distribution before failure, we can see that both symmetry design and ductile mode structures have distributed stress fields, leading to relatively high strength in both cases. But there exist some differences in toughness due to the spatial positions of the stress within the structure. The design space of our current study is expected to be larger compared to graded designs and can therefore potentially lead to better performances. We have tested a graded design under compression and the resultant stress–stain curves, and the failure be found in the Supporting Information Figure S6. In addition, the proposed structure is applicable to a wide range of fabrication approaches including polyjet and SLA which are capable of prototyping complex geometry proposed in our work with high efficiency and accuracy compared to other conventional methods. To realize such designs, a combined computational and experimental framework with additive manufacturing is used to study beam element radius effects.

Correlation Analysis and Optimization. To investigate the relationship of the design parameters and the performance of the structures, we plot the strength with respect to the mean radii and the standard deviation of the 8 randomly generated beams and the radii of the off-diagonal beams (Figure 4(A)). The figure shows that the data are heterogeneous with different levels of correlations. Strength increases as the mean radius of the beams along the designed diagonal increases since larger radii raise the abilities of the diagonal beams to bear the resultant shear force. But, due to the volume fraction constraint, the thicker the designed diagonal beams are, the thinner the rest of the beams are. This results in a negative correlation as the mean beam radius exceeds 1.1 mm when the structures fail along other fracture surfaces. The inverse trend can be observed in the radii of the off-diagonal beams due to the fixed volume fraction. To better understand how the design parameters affect the mechanical performances of the structures, we plot the correlation between the input parameters (Figure 4(B)), (i) mean and (ii) standard deviation of the 8 randomly assigned beams, (iii) radii of the off-diagonal beams, and the (iv) number of the unique orientations of the unit cells along the diagonal, and three target mechanical properties, strength, stiffness, and toughness. The results shown in the bar graph indicate that there are also high positive correlations between the mean radii of the 8 beams and stiffness and toughness. On the contrary, the radii of the off-diagonal beams have high negative correlation with

https://doi.org/10.1021/acsmaterialslett.3c00002
ACS Materials Lett. 2023, 5, 1288–1294

strength, stiffness, and toughness. Therefore, the optimal designs can be found by balancing the magnitudes of beam radii at those locations. Moreover, standard deviation of the 8 beam radii and the number of unique orientations of the unit cells have lower correlation with the target mechanical properties.

With the understanding of the failure mechanisms behind the designs, we then aim to optimize the beam arrangement of the design to obtain structures with higher strength and toughness. The formulation of the design process can be written as an optimization problem with mixed variables (eq 1) where the objective is a linear combination of the toughness and strength, which can vary to accommodate different applications but here we use cost function $\pi_{cost} = 1 \times$ strength $+10 \times$ toughness to validate the approach, subject to a constraint for fixing the volume fraction.

$$\max_{r_i, s_i} f_{sim}(r_i, s_i)$$

$$\text{s.t.} \sum_{1}^{R} \frac{a^3}{8} \times \left[3\sqrt{3}\pi\left(\frac{r_i}{L}\right)^2 - 18\sqrt{2}\left(\frac{r_i}{L}\right)^3\right] = 0.2$$

$$0.5 \le r_i \le 1.7$$

$$s_i \in \{1, 2, ..., 6\} \quad (1)$$

where R is the total number of the beams within a structure, which is 4096 in our case since there are 8 beams in a unit cell and 512 (8 by 8 by 8) BC unit cells in the entire structure. To fabricate the structures within manufacturing resolutions, the beam radii, r_i, are set between 0.5 and 1.7 mm, while s_i are discrete variables representing unit cell orientations along the diagonal. The objective is a finite element model mapping the design parameters to the structures' performances. Since the objective cannot be written as an analytical solution, a constrained Bayesian optimization is then established to find the optimum. The results obtained from the correlation analysis shows that the orientations of the unit cells have low correlation to the mechanical performance so the variables we are interested in are only the 8 beam radii that are randomly drawn from the uniform distribution. In the optimization process, the set of orientations of the best design sampled from the uniform distribution are adopted. After that, the algorithm fixes the orientations of all designs throughout the process and only optimizes over the beam radii. The implementation details are illustrated in Figure 5(A) and included in the Methods Section. Figure 5(B) shows the designs proposed by the optimization algorithm. From the heatmaps of the beam radii, we can see that the beams along the diagonal in both designs are thicker than the rest of the beams to bear the resultant shear. If looking closer at the arrangement of the beams, we can see that the beams perpendicular to the fracture surface are thicker than the beams positioned along the diagonal. The reason behind this is that the beams are designed to hold axial loading, so the beams aligned with the fracture surface are less critical and require less material. In addition, the contact pressure of the designs during the compression are also plotted in Figure 5(B) showing that both structures fail at the boundaries and the cracks grow locally without penetrating through the entire structure, leading to more progressive failure, following the ductile failure mode discussed before. We also plot the stress−strain curves of both designs and compare the results with the conventional symmetric design. From the plot, we can see that the proposed designs can still withstand

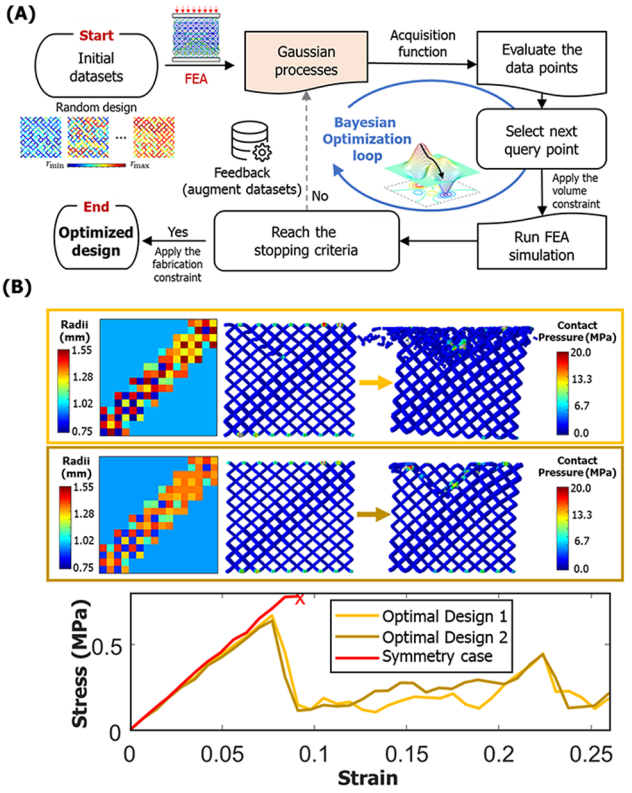

Figure 5. (A) The flowchart of simulation-based Bayesian optimization process. (B) The stress−strain curves of the optimal designs and the symmetric structure, showing the optimal designs have more progressive failure and better mechanical performances. Contact pressure is magnitude of the net contact normal force per unit area with unit MPa.

some external load during the failure process. The overall combined performance improves 9.96% compared to baseline (symmetric case) with a 16.4% drop in strength but 112.6% increase in toughness. Even though improperly designed asymmetric structures may have worse performance than symmetric ones, the results show that the optimization algorithm eliminates the potential possibility of having catastrophic failure, resulting in more ductile designs.

In this study, we propose a method to create asymmetric strut-based BC cellular structures with improved toughness and more progressive failure. The beam radii near the diagonal fracture surface are modified, as they have a greater influence on the performance, to create asymmetry. Next, explicit finite element simulations are established to numerically calculate the homogenized mechanical properties of the entire structures. The samples are drawn using CAD and fabricated with SLA 3D printers to verify the simulation results. Three failure modes, including brittle mode, transition, and ductile mode, are identified in the data drawn from uniform distributions. We also calculate the correlations between the input variables and the target material properties. Lastly, we formulate the design process into a maximum optimization problem and perform simulation-based Bayesian optimization to approximate and solve the objective function, simultaneously. This data-efficient online optimization approach allows us to obtain optimal designs without generating massive data sets and to solve problems requiring complex evaluation processes. The algorithm-proposed designs have significantly

https://doi.org/10.1021/acsmaterialslett.3c00002
ACS Materials Lett. 2023, 5, 1288−1294

higher toughness with little sacrifice in strength compared to the conventional symmetric design. This study can further be broadened to accommodate various applications with specific property requirements by tailoring the weights of different mechanical properties in the objective function and introducing more variables to expand the design space for improved properties and achieve programmable local deformation and densification.

METHODS

Dynamic Numerical Simulations. In this paper, finite element simulations of cellular structures under compression are performed using Abaqus Explicit with automatic time step, which determines the size of time step based on numerically stability, to predict the homogenized stress and strain of the structures under compressive loading. The use of dynamic models allows us to obtain the configurations of the structures during their failure. Timoshenko beam elements are used in the simulations, and the material model with the Young's modulus of 2000 MPa, Poisson's ratio of 0.33, yield stress of 65 MPa, density of 1.15×10^{-9} tonne/mm^3, and fracture strain of 0.0001 is used in every simulation. To account for the boundary effects for beam elements, we increase the yield strength near the boundary to 80 MPa to avoid unrealistic material failure due to geometric singularity of beam elements in FEA, details are provided in the Supporting Information Figure S7. A displacement of 0.35a, where a represents the unit cell length in mm, is applied in the negative y-direction while the bottom surface of the structure is fixed during the entire simulation process. The total simulation time length is 0.08 s, leading to a world clock time length of around 2 h. The simulation settings in the 100-parameter design space are validated with the experiments of the symmetric cellular and asymmetric cellular structures.

Correlation Analysis and Simulation-Based Bayesian Optimization. Correlation analysis is performed to extract the features that are more crucial to the desired properties and to better understand the mechanics of the proposed structures. Four input parameters (mean and standard deviation of the 8 randomly assigned beams, radii of the off-diagonal beams, and the number of the unique orientations of the unit cell along the diagonal) are used in the analysis. We calculate the correlation between these input parameters and strength, stiffness, and toughness, leading to a total of 12 combinations. Based on this analysis, we can extract the features with the greatest influence on the performance to establish simulation-based Bayesian optimization to determine the optimal design. Bayesian optimization is a black-box optimization technique for determining the optimal point over an unknown objective with limited data points. The objective in this design problem is the function mapping the design space to the performance space, which is difficult to be explicitly governed by an equation. To tackle the unknown objective, this optimization process will first approximate the objective function by forward regression, and search for the optima by backward process. This optimization process will be iterated until a better design is achieved. In terms of the forward regression, Gaussian process regression is adopted to create a surrogate model under the assumption that any function can be approximated by an infinite dimensional multivariate Gaussian distribution. After the forward regression process, we can obtain a function that goes through all the existing data points and approximates the performances of the unknown ones. During the backward process, acquisition functions are used to sample the points closer to the optima that have larger impacts on determining a representative model in the next forward regression process. In this paper, the probability of improvement, one of the commonly used acquisition functions, is adopted to evaluate the probability of the current state being improved to get the next query point. Another acquisition function: expected improvement is also tested in the process to maximize the expected improvement over the current best.[21−23] The volume fraction constraint is then applied on the proposed query point to build a reasonable structure and evaluate the performance of the structure by running the compression test in simulator. The design is then added to the initial data set to reevaluate and augment the surrogate model. In this paper, we iterate the process 50 times and select the points that satisfy the fabrication constraint and that perform with high objective value as well as being the optimal points. The use of this approach is essential to significantly reduce the computational cost needed in the optimization process since the simulation in this study is relatively complex and computationally expensive.

Fabrication and Experiments. The asymmetric cellular structures are modeled using scripts in AutoCAD LISP and 3D printed with the Form 3 SLA printer developed by Formlabs using standard resin. The printer selectively cures the liquid polymer resin layer-by-layer via an ultraviolet laser beam with a thickness of 50 μm. To accurately fabricate the samples and avoid the interference of the structures, the maximum and minimum beam radii of the printed samples are set to 1700 and 500 μm, respectively, as a design constraint. The design domain of interest has a total of 512 unit cells ($8 \times 8 \times 8$) for the entire structure. We conduct uniaxial quasi-static compression tests using displacement control with a loading speed of 5 mm/min resulting in a strain rate of about 1.04×10^{-3} /s. To take the effect of the beam radii into account, we position the structures to make the orientations consistent across CAD models, numerical simulations, and experiments for each sample.

ASSOCIATED CONTENT

Supporting Information

The Supporting Information is available free of charge at https://pubs.acs.org/doi/10.1021/acsmaterialslett.3c00002.

Simulation-based Ashby chart comparing different numbers of asymmetric cellular samples, the effect of different threshold values on the performances of the designs, experimental results of graded design, and the cross-sectional areas of the beams of the fabricated samples (Figures S1, S2, S6, and S7), the snapshots of the simulation of the designs under compression loads (Figures S3−S5) (PDF)

AUTHOR INFORMATION

Corresponding Author

Grace X. Gu − *Department of Mechanical Engineering, University of California, Berkeley, California 94720, United States;* orcid.org/0000-0001-7118-3228; Email: ggu@berkeley.edu

Authors

Shao-Yi Yu − *Department of Mechanical Engineering, University of California, Berkeley, California 94720, United States*

https://doi.org/10.1021/acsmaterialslett.3c00002
ACS Materials Lett. 2023, 5, 1288−1294

Sangryun Lee − *Department of Mechanical Engineering, University of California, Berkeley, California 94720, United States; Division of Mechanical and Biomedical Engineering, Ewha Womans University, Seoul 03760, South Korea*
Zhizhou Zhang − *Department of Mechanical Engineering, University of California, Berkeley, California 94720, United States*
Zeqing Jin − *Department of Mechanical Engineering, University of California, Berkeley, California 94720, United States*

Complete contact information is available at: https://pubs.acs.org/10.1021/acsmaterialslett.3c00002

Author Contributions

CRediT: **Shao-Yi Yu** data curation, formal analysis, investigation, methodology, writing-original draft; **Sangryun Lee** formal analysis, methodology, writing-review & editing; **Zhizhou Zhang** formal analysis, investigation, writing-review & editing; **Zeqing Jin** formal analysis, investigation, writing-review & editing; **Grace X. Gu** conceptualization, formal analysis, investigation, writing-original draft.

Notes

The authors declare no competing financial interest.

■ ACKNOWLEDGMENTS

This research was supported by Office of Naval Research (Fund Number: N00014-21-1-2604), Army Research Office (Fund Number: W911NF-22-1-0175), and National Science Foundation XSEDE Supercomputing Resources (Fund Number: ACI-1548562).

■ REFERENCES

(1) Gibson, L. J. Cellular Solids. *MRS Bull.* **2003**, *28*, 270−274.
(2) Liu, K.; Sun, R.; Daraio, C. Growth rules for irregular architected materials with programmable properties. *Science* **2022**, *377*, 975−981.
(3) Lee, S.; Zhang, Z.; Gu, G. X. Generative machine learning algorithm for lattice structures with superior mechanical properties. *Materials Horizons* **2022**, *9*, 952−960.
(4) Fazekas, A.; Dendievel, R.; Salvo, L.; Bréchet, Y. Effect of microstructural topology upon the stiffness and strength of 2D cellular structures. *International Journal of Mechanical Sciences* **2002**, *44*, 2047−2066.
(5) Limmahakhun, S.; Oloyede, A.; Sitthiseripratip, K.; Xiao, Y.; Yan, C. Stiffness and strength tailoring of cobalt chromium graded cellular structures for stress-shielding reduction. *Materials & Design* **2017**, *114*, 633−641.
(6) Chen, C.-T.; Chrzan, D. C.; Gu, G. X. Nano-topology optimization for materials design with atom-by-atom control. *Nat. Commun.* **2020**, *11*, 3745.
(7) Ma, Q.; Rejab, M. R. M.; Siregar, J. P.; Guan, Z. A review of the recent trends on core structures and impact response of sandwich panels. *Journal of Composite Materials* **2021**, *55*, 2513−2555.
(8) Munsch, M. In *Laser Additive Manufacturing*; Brandt, Milan, Ed.; Woodhead Publishing, 2017; pp 399−420.
(9) Al-Ketan, O. Programmed plastic deformation in mathematically-designed architected cellular materials. *Metals* **2021**, *11*, 1622.
(10) Ajdari, A.; Nayeb-Hashemi, H.; Vaziri, A. Dynamic crushing and energy absorption of regular, irregular and functionally graded cellular structures. *International Journal of Solids and Structures* **2011**, *48*, 506−516.
(11) Raghavendra, S.; et al. Quasi-static compression and compression−compression fatigue behavior of regular and irregular cellular biomaterials. *Fatigue & Fracture of Engineering Materials & Structures* **2021**, *44*, 1178−1194.
(12) Mukhopadhyay, T.; Adhikari, S. Equivalent in-plane elastic properties of irregular honeycombs: An analytical approach. *International Journal of Solids and Structures* **2016**, *91*, 169−184.
(13) Liu, C.; Lertthanasarn, J.; Pham, M.-S. The origin of the boundary strengthening in polycrystal-inspired architected materials. *Nat. Commun.* **2021**, *12*, 4600.
(14) Pham, M.-S.; Liu, C.; Todd, I.; Lertthanasarn, J. Damage-tolerant architected materials inspired by crystal microstructure. *Nature* **2019**, *565*, 305−311.
(15) Han, Y.; Lu, W. F. A Novel design method for nonuniform lattice structures based on topology optimization. *Journal of Mechanical Design* **2018**, *140*, 091403.
(16) Al-Saedi, D. S. J.; Masood, S. H.; Faizan-Ur-Rab, M.; Alomarah, A.; Ponnusamy, P. Mechanical properties and energy absorption capability of functionally graded F2BCC lattice fabricated by SLM. *Materials & Design* **2018**, *144*, 32−44.
(17) Bai, L. Mechanical properties and energy absorption capabilities of functionally graded lattice structures: Experiments and simulations. *Int. J. Mechanical Sci.* **2020**, *182*, 105735.
(18) Nguyen, C.; Peetz, D.; Elbanna, A. E.; Carlson, J. M. Characterization of fracture in topology-optimized bioinspired networks. *Phys. Rev. E* **2019**, *100*, 042402.
(19) Kadic, M.; Bückmann, T.; Schittny, R.; Gumbsch, P.; Wegener, M. Pentamode Metamaterials with independently tailored bulk modulus and mass density. *Physical Review Applied* **2014**, *2*, 054007.
(20) Jang, W.-Y.; Kyriakides, S. On the crushing of aluminum open-cell foams: Part I. Experiments. *International Journal of Solids and Structures* **2009**, *46*, 617−634.
(21) Snoek, J.; Larochelle, H.; Adams, R. P. Practical Bayesian optimization of machine learning algorithms. *Advances in neural information processing systems* **2012**, *25*, 313.
(22) Kushner, H. J. A new method of locating the maximum point of an arbitrary multipeak curve in the presence of noise. *Journal of Basic Engineering* **1964**, *86*, 97−106.
(23) Frazier, P. I. A tutorial on Bayesian optimization. *arXiv preprint doi* **2018**, DOI: 10.48550/arXiv.1807.02811.